Title	Surface finishing method using plasma chemical vaporization machining for narrow channel walls of x-ray crystal monochromators
Author(s)	Hirano, Takashi; Morioka, Yuki; Matsumura, Shotaro et al.
Citation	International Journal of Automation Technology. 2019, 13(2), p. 246-253
Version Type	VoR
URL	https://hdl.handle.net/11094/86957
rights	This article is licensed under a Creative Commons Attribution-NoDerivatives 4.0 International License.
Note	

Paper:

Surface Finishing Method Using Plasma Chemical Vaporization Machining for Narrow Channel Walls of X-Ray Crystal Monochromators

Takashi Hirano[*],[†]**, Yuki Morioka**[*]**, Shotaro Matsumura**[*]**, Yasuhisa Sano**[*]**, Taito Osaka**[**]**,
Satoshi Matsuyama**[*]**, Makina Yabashi**[**]**, and Kazuto Yamauchi**[*]

[*]Department of Precision Science and Technology, Graduate School of Engineering, Osaka University
2-1 Yamada-oka, Suita, Osaka 565-0871, Japan
[†]Corresponding author, E-mail: hirano@up.prec.eng.osaka-u.ac.jp
[**]SPring-8 Center, RIKEN, Sayo, Japan

Channel-cut Si crystals are useful optical devices for providing monochromatic X-ray beams with extreme angular stability. Owing to difficulties in the high-precision surface finishing of narrow-channel inner walls of the crystals, typical channel-cut crystals have considerable residual subsurface crystal damage and/or roughness on their channel-wall reflection surfaces that decrease intensity and distort the wavefronts of the reflected X-rays. This paper proposes a high-precision surface finishing method for the narrow-channel inner walls based on plasma chemical vaporization machining, which is a local etching technique using atmospheric-pressure plasma. Cylinder- and nozzle-shaped electrodes were designed for channel widths of more than 5 and 3 mm, respectively. We optimized process conditions for each electrode using commercial Si wafers, and obtained a removal depth of 10 μm with a surface flatness and roughness of less than 1 μm and 1 nmRMS, respectively, which should allow the damaged layers to be fully removed while maintaining the wavefront of coherent X-rays.

1. Introduction

Intense, coherent, and ultrashort X-ray pulses from X-ray free-electron lasers (XFELs) [1, 2] and next-generation diffraction-limited storage rings (DLSRs) have opened up unprecedented and entirely new possibilities for revealing physical structures, dynamics, and chemical states of diverse systems in the atomic scale. In most X-ray experiments, beam conditioning with crystal monochromators, which consist of perfect single crystals such as silicon, is important owing to the broad spectral width of the X-rays emitted from these synchrotron sources. An X-ray diffraction process by the crystal acts as both a bandpass filter and a mirror; they can produce well-defined narrow-band X-rays without undesired spectral contamination, while deflecting the beam axis. A photon energy E of the diffracted X-rays is determined by Bragg's law as

$$E = \frac{hc}{\lambda} = \frac{hc}{2d\sin\theta_{\mathrm{B}}}, \qquad \ldots \ldots \ldots \ldots \quad (1)$$

where h, c, λ, d, and θ_{B} denote the Plank constant, the speed of light, the wavelength, the lattice spacing of crystal, and the kinematical Bragg angle, respectively. Typically, the relative bandwidth of diffracted X-ray spectra becomes narrower at a smaller d in a given material. A high-order diffraction plane with a small d is preferred for spectroscopy experiments that require high energy resolution [3, 4], while a low-order diffraction plane with a large d such as Si(111) is useful for achieving a high flux with a reasonable bandwidth.

Double-crystal monochromators (DCMs), which are composed of a pair of Si(111) crystals, have been widely used as standard monochromators in the hard X-ray beamlines of the synchrotron facilities because the beam direction can be preserved. Since a sophisticated high-quality surface finishing technique can be applied to every crystal surface, DCMs have geometrically and crystallographically well-defined reflection surfaces, which enables ideal X-ray diffraction. The high flexibility in the position of each crystal allows it to cover a wide range of photon energies for various X-ray applications. For example, the standard Si(111) DCM at the Japan's XFEL facility, SACLA, covers a photon energy range of 4–30 keV [5]. However, such multiple crystal arrangements suffer from the independent mechanical vibrations of separate crystals [6, 7]. The angular instabilities cause fluctuation in the beam position at the sample and decrease in coherent flux.

The use of channel-cut crystal monochromators (CCMs), which are monolithic optical devices with two inner-wall reflection surfaces in a single crystal block, is highly useful for obtaining stable monochromatic X-rays
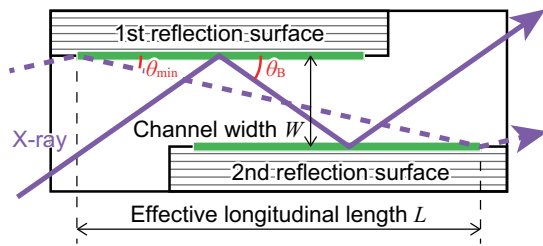
Fig. 1. Channel-cut crystals. Effective reflection areas are highlighted by the green lines.

(**Fig. 1**) [8, 9]. The beam direction is accurately preserved after two-bounce reflections at the two inner-wall surfaces with parallel lattice planes in a single crystal [6, 10]. However, it has been difficult to realize ideal X-ray diffraction with CCMs, due to difficulty in achieving the high-quality surface finishing of the internal side walls with conventional polishing- and etching-based techniques. Polishing techniques introduce subsurface crystal damage [10], while etching induces considerable surface roughness and undulation [11]. These imperfections distort the wavefront, which generates intensity modulation (so-called speckle), and also decrease the intensity of the exit beam.

To fabricate speckle-free CCMs, we have developed a high-precision surface finishing method based on plasma chemical vaporization machining (PCVM) [12–15]. It is a purely chemical etching technique using atmospheric-pressure plasma, which results in a crystallographically damage-free process. Also, the use of fluoride molecules as an etchant gas enables isotropic removal of Si atoms for all lattice planes, owing to the high reactivity of the fluorine radical [16]. We have already confirmed that a PCVM-based method using a cylindrical electrode with a diameter of 10 mm ($\phi10$) can produce flat and smooth surfaces with high crystal perfection. Then we obtained speckle-free reflection profiles for XFEL beams by using PCVM-finished Si(220) CCMs with a channel width W of 30 mm [15], which has been used in a hard X-ray split-and-delay optical system [17–19].

On the other hand, the photon-energy range of CCM is limited by the fixed arrangement of the reflection surfaces as follows;

$$\frac{hc}{2d \sin \theta_{max}} < E < \frac{hc}{2d \sin \theta_{min}}, \quad \ldots \ldots \quad (2)$$

where θ_{max} (θ_{min}) is the maximum (minimum) incident angle. In particular, θ_{min} is limited by the effective longitudinal length L and the channel width W as shown in **Fig. 1**. To cover $E = 30$ keV with Si(111) CCMs, $W < 8$ mm is required with a reasonable length $L \sim 120$ mm, for which a conventional PCVM system using the $\phi10$ electrode is not available.

In this study, we extended the capability of the inner-wall PCVM method to CCMs with $W < 8$ mm, using two types of smaller electrodes. We present the processing characteristics of the inner-wall PCVM method for each electrode. We investigated scanning methods to obtain flat

and smooth surfaces at a target removal depth. Also, we analyzed the dependence of the PCVM process on the lattice plane of Si crystal, which is important for processing crystal optical devices that require a variety of the lattice planes. Although the isotropic nature of the PCVM process for the Si crystals was confirmed empirically [13, 15], a quantitative analysis of the dependence has not been reported.

2. Target Properties and Fabrication System

A conventional polishing-based process is used as a pre-process before surface finishing via PCVM for CCMs to produce highly flat surfaces. The target removal depth of the PCVM process is thus about 10 μm, to completely eliminate the damaged layers induced by the pre-process, which comprise a thickness of several micrometers (comparable to a size of the slurry particles). The surface undulation should be sufficiently smaller than 1 μm in order not to distort reflection XFEL profiles in space and time [15]. Whereas micro-roughness in the surface structure hardly affects the X-ray diffraction, surface roughening in the PCVM process indicates re-deposition of reaction products, which can deteriorate reflection X-ray properties. The target roughness of the finished surface is less than 1 nmRMS, similar to that of high-quality polished surfaces. Also, the processing area, corresponding to the spatial acceptance of the CCMs, should be much larger than the typical beam size of ∼0.5 mm for XFELs [5] and a few millimeters for DLSRs.

Figure 2 shows schematics of the inner-wall PCVM equipment for CCMs with the narrow channel. The vacuum chamber is filled with a high-purity gas after evacuating ambient air to a pressure of 10^{-4} Pa. The plasma is generated between the target inner wall and the electrode inserted into the channel under atmospheric pressure. The CCM is mounted on a grounded X-Y stage while the electrode moves along the Z-axis, which allows us to adjust the processing area and the gap between the target inner wall and the electrode. To avoid unintended processing, the electrode should be apart from all surfaces (except the target inner wall) by > 1 mm.

We first designed a cylindrical electrode with a minimum diameter. A line plasma is generated with the cylindrical electrode under a surrounding gas of He/SF$_6$ as shown in **Fig. 2(a)**. The electrode height was 8 mm for efficient processing of whole inner-wall surfaces via uniaxial scanning with the line plasma of a comparable length. The diameter of the thinnest part of the shaft was 2 mm, to ensure the stiffness of the electrode during the high-speed rotation that produces a fast laminar gas flow in the gap as shown in **Fig. 2(c)**; this is important for achieving a high removal rate and surface smoothness [15]. Considering the 1 mm gap added to prevent the generation of the plasma between the inner wall and the shaft, it was decided that the diameter of the electrode should be 4 mm ($\phi4$), which is applicable to CCMs with $W > 5$ mm.
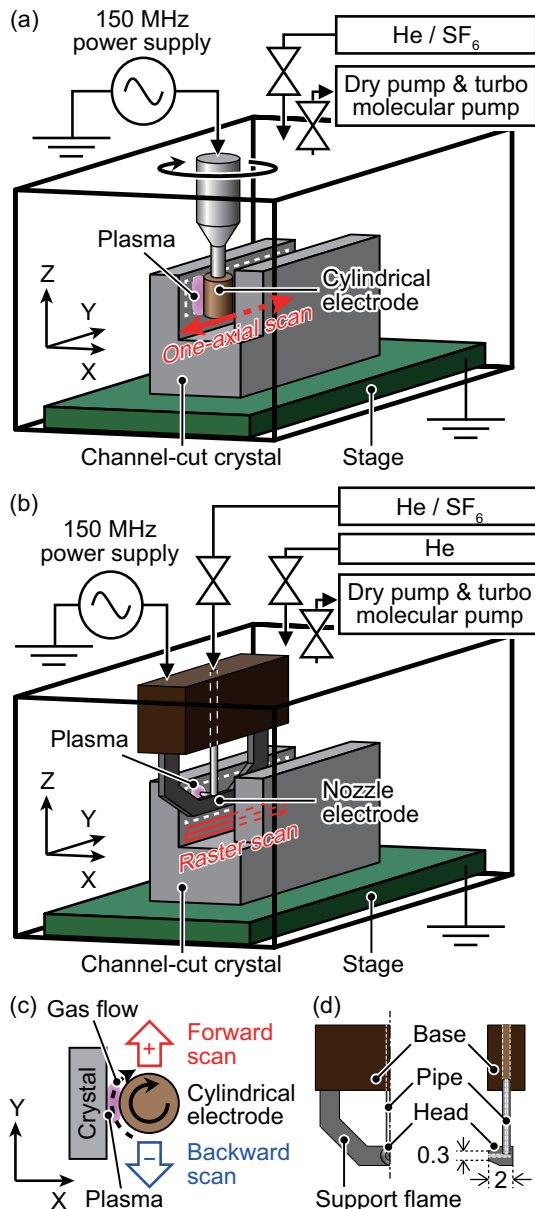
Also, to accommodate narrower channels with $W <$

Fig. 2. Equipment for surface finishing of channel-cut crystals using (a) cylindrical and (b) nozzle electrodes. (c) Directions of rotation of the cylindrical electrode and a scan direction. A forward scan is a scan performed in the same direction as the gas flow produced by the rotation. (d) Schematics of the nozzle electrode with a right-angled nozzle head. Units of dimensions are millimeters.

5 mm, we developed a nozzle electrode using a gas introduction system with a right-angled nozzle head. The etching gas of He/SF$_6$ is delivered to the nozzle head through a pipe parallel to the inner wall with outside and inside diameters of 0.5 mm and 0.2 mm, respectively. The plasma is generated between the inner wall and the nozzle head under a surrounding gas of He (**Fig. 2(b)**). A support frame with a thickness of 1 mm was used to ensure the stiffness of the electrode. The minimum total depth of the electrode was thus 2 mm as shown in **Fig. 2(d)**, which can be applied to $W > 3$ mm. Additionally, the small diameter

Table 1. Typical experimental conditions.

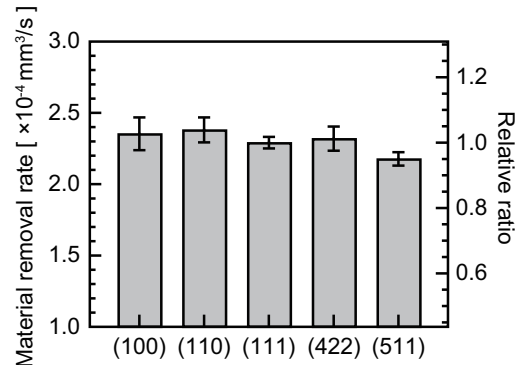|	
Ambient gas pressure	100 kPa
Ratio of etching gas	He : SF$_6$ = 99.5 : 0.5
Gap between sample and electrode	0.2–0.3 mm
Electric power	∼15 W

Fig. 3. Dependences of material removal rate on lattice plane of Si crystal. The removal rate for each lattice plane was calculated from an area of a cross-sectional removal profile using a uniaxial scan with a scan speed of 10 mm/min. The error bars represent standard deviations of six experiments.

of the nozzle head of 0.3 mm can localize the plasma area to a sub-mm size, which is useful for correcting figure errors with computer-controlled scan speeds. The whole target areas are processed by two-axis raster scanning of the plasma.

3. Processing Characteristics

Processing characteristics of the inner-wall PCVM with each electrode were investigated using commercial Czochralski (CZ)-Si(110) wafers with a roughness value of ∼0.2 nmRMS. In this basic test, the sample wafer was fixed vertically to represent the channel walls. Cross-sectional surface profiles and roughness values in 187×140 μm^2 of the processed area were measured with a microscopic interferometer (Zygo, NewView 7100).

Typical experimental conditions in the PCVM process are listed in **Table 1**. A high ratio of He in the etching gas was important for generating highly stable and uniform plasma at an atmospheric pressure of 100 kPa. The narrow gap contributed to the generation of the laminar flow with a high flow rate of several millimeters per second. An electric power input was minimized to avoid supplying excess energy to the charged particles in the plasma.

3.1. Lattice Plane Dependence

In addition to Si(110) wafers, (100), (111), (422), and (511) wafers were prepared to study the dependence on the lattice plane. For each wafer, **Fig. 3** shows averaged
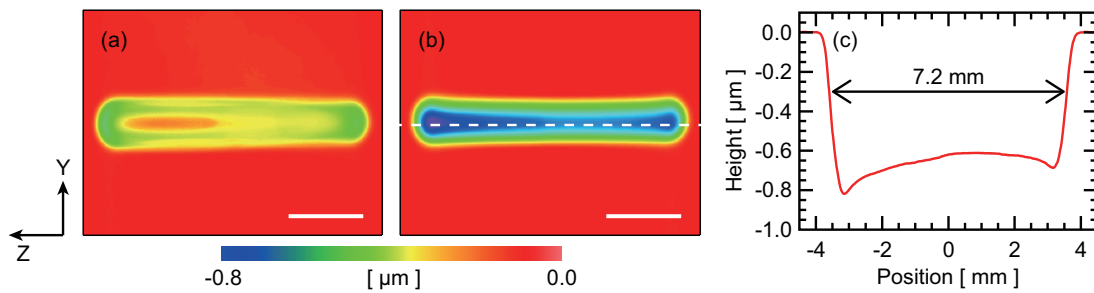
Fig. 4. Removal footprints of the cylindrical electrode at rotation speeds of (a) 0 rpm and (b) 6000 rpm, and a processing time of 10 s. Vertical direction is the scanning axis. The scale bars represent a length of 2 mm. (c) Cross-sectional line profile along white dashed line in (b).

material removal rates (MRRs) of six removals performed using the conventional PCVM system [13]. Here, the MRR is defined as

$$\text{MRR} = S_{\text{ave}} \times v, \quad \dots \dots \dots \dots \quad (3)$$

where S_{ave} and v denote the averaged area of cross-sectional profiles and the scan speed of the plasma. The differences in the MRR ratio $((100) : (110) : (111) = 1.03 : 1.04 : 1.00)$ were negligible compared to those with alkaline-solution etching $((100) : (110) : (111) = 100 : 160 : 1)$ reported in [20]. The maximum difference in MRR among these lattice planes, 8.5%, was not significantly larger than the averaged relative standard deviation of 3.2%, which not only indicates the capability to obtain similar removal profiles for arbitrary lattice planes including Si(111), but also to produce highly flat and smooth surfaces without etch pits.

3.2. Cylindrical Electrode

Figure 4 shows static removal profiles with different rotation speeds of the $\phi 4$ electrode at a processing time of 10 s. At a rotation speed of 0 rpm, the hollow removal profile was formed as shown in **Fig. 4(a)**, because the etching gas supplied by diffusion from the surroundings was mostly consumed at the outer region of the plasma. On the other hand, the uniform line-shaped profile shown in **Fig. 4(b)** was obtained at a rotation speed of 6000 rpm, owing to the introduction of sufficient amounts of gas into the center region of the plasma. The asymmetric cross-section profile along the Z-axis shown in **Fig. 4(c)** was formed because of the variation in the gap caused by warpage in the wafer or the tilt of the rotation axis of the electrode. The larger removal depth around the ± 3 mm positions in **Fig. 4(c)** was due to higher amount of the gas supply from the surroundings at the outer region of the plasma. The MRR with the rotation speed of 6000 rpm was estimated to be 4.1×10^{-4} mm^3/s. As shown in **Fig. 4(c)**, the length of the removal profile was 7.2 mm in full-width at half-maximum (FWHM), which satisfies the requirement on the spatial acceptance.

Figure 5 shows the dependence of the removal depth and roughness on the rotation speed, i.e., a peripheral speed, of both $\phi 4$ and $\phi 10$ electrodes at a scan speed of 20 mm/min. The scan direction was the same as that of
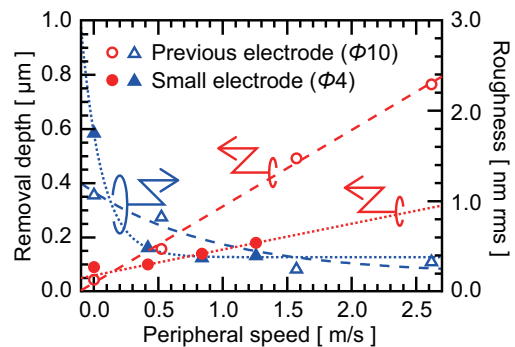

Fig. 5. Dependences of removal depth and roughness on rotation speed of the cylindrical electrodes. The results using the previous and small electrodes with diameters of 10 and 4 mm are plotted as open and closed marks, respectively. Circles and triangles represent removal depths and roughness values, respectively.

the laminar flow, which is referred to as a forward scan (**Fig. 2(c)**). The maximum rotation speed of the electrode was 6000 rpm, corresponding to peripheral speeds of 1.26 m/s and 3.14 m/s for the $\phi 4$ and $\phi 10$ electrodes, respectively. The removal depths increased linearly with the peripheral speed, indicating that the supplying rate of the etchant is a bottleneck in the PCVM reaction within these peripheral-speed ranges. Downsizing the electrode from $\phi 10$ to $\phi 4$ reduced the laminar flow rate and processing area along the scan direction, resulting in a reduced removal rate. A smooth surface with a roughness of ~ 0.4 nmRMS was achieved even with the $\phi 4$ electrode at the higher rotation-speed range, since the peripheral speed of > 1 m/s was sufficient for preventing re-deposition on the nearby surfaces.

The optimal scanning method for achieving the target removal depth was discussed. In the previous study, we found that a single forward scan method with a scan speed slowed down to 1–10 mm/min caused surface roughening for increased removal depth, while a multiple forward scan method with a high scan speed of > 10 mm/min generated smooth surfaces over a wide range of removal depths, owing to the small surface roughness introduced by one high-speed scan and the decrease in roughness dur-
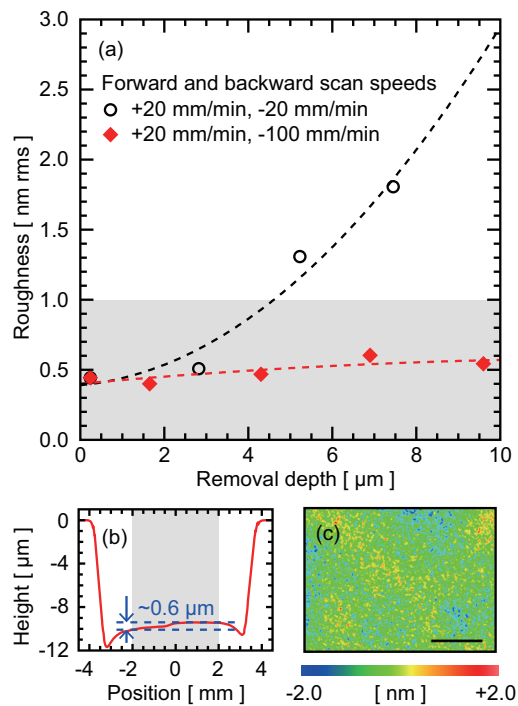
Fig. 6. (a) Averaged surface roughness as a function of removal depth in multiple forward and reciprocal scan methods using the cylindrical electrode. A target roughness value of < 1 nmRMS is highlighted in gray. (b) Cross-sectional line profile and (c) surface morphology at a removal depth of 9.6 μm in the reciprocal scan method with scan speeds of 20 and 100 mm/min in forward and backward scans, respectively. The scale bar in (c) represents a length of 50 μm. The peak-to-valley value of the center 4-mm-width area, highlighted in gray, is 646 nm. The roughness value is 0.508 nmRMS (4.453 nm in peak-to-valley).

ing the following scans [15]. In this study, we proposed a reciprocal scan method employing high-speed forward scans and much higher-speed backward scans. With a backward scan speed of 100 mm/min, the surface roughening can be successfully suppressed to < 0.6 nmRMS, as shown in **Fig. 6(a)**. At a removal depth of ∼10 μm, the surface undulation and roughness of the processed area were 0.6 μm in peak-to-valley (PV) and 0.5 nmRMS, as shown in **Figs. 6(b)** and **(c)**, respectively, which satisfied the target values. Conversely, the reciprocal scan method with the constant forward and backward scan speeds resulted in intolerable surface roughness at a removal depth of > 5 μm, as shown in **Fig. 6(a)**. This is because the backward scan, in which the reaction products flow out to the side of the finished surface, caused higher amounts of re-deposited contaminations compared to the forward scan with the same scan speeds. Note that in PV, the roughness value tendencies associated with the removal depth were similar to those in RMS for all experiments.

3.3. Nozzle Electrode

Figure 7 shows a static removal profile formed using the nozzle electrode with a gas-volume flow rate of
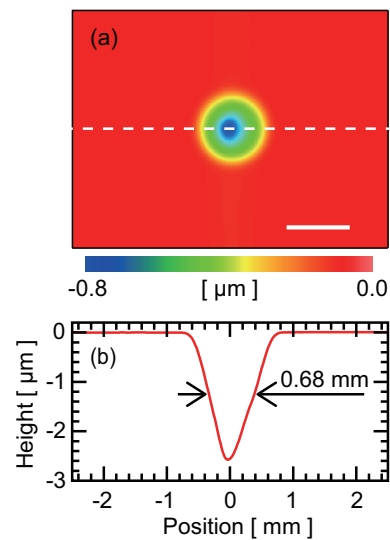

Fig. 7. (a) Removal footprint of the nozzle electrode with a gas-flow rate of 100 sccm and a processing time of 15 s. The scale bars represent a length of 2 mm. (b) Cross-sectional line profile along white dashed line in (a).
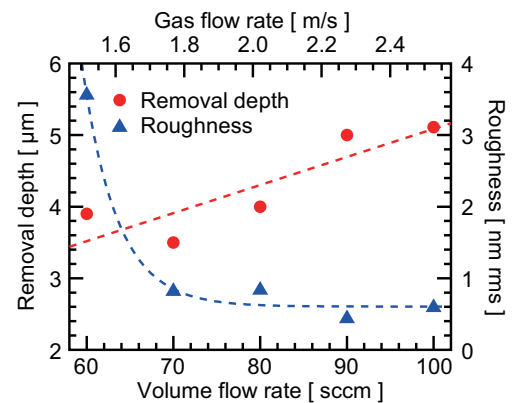

Fig. 8. Dependences of removal depth and roughness on gas-flow rate of the nozzle electrode. The gas-flow rate was calculated from the gas volume passing through the side surface of a cylinder with a diameter and a height of 0.7×0.3 mm per unit time, which corresponds to the width of the plasma and the gap between the sample and the electrode.

100 sccm at a processing time of 15 s. An isotropic Gaussian-shaped profile with a small size of 0.68 mm in FWHM was obtained. The MRR was 8.6×10^{-5} mm^3/s, which is five times lower than that of the cylindrical electrode.

Figure 8 shows the gas-flow rate dependence on the removal depth and roughness after raster scans at a scan speed of 20 mm/min. The removal rate and surface smoothness were improved for increased gas flow rate, similar to the results shown in **Fig. 5**.

Finally, we performed two-axis raster scanning of a 3×3 mm^2 area with the nozzle electrode to investigate roughness dependence on the removal depth. **Fig. 9(a)** shows results of two independent experiments at the same gas-
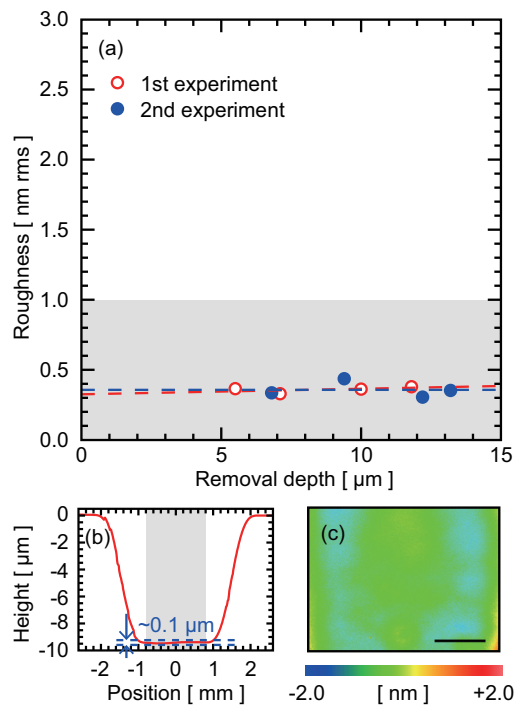
Fig. 9. (a) Averaged surface roughness as a function of removal depth using the nozzle electrode. A target roughness value of < 1 nmRMS is highlighted in gray. (b) Cross-sectional line profile and (c) surface morphology at a removal depth of 9.4 μm. The scale bar in (c) represents a length of 50 μm. The peak-to-valley value of the center 1.6-mm-width area, highlighted in gray, is 97.2 nm. The roughness value is 0.363 nmRMS (3.183 nm in peak-to-valley).

volume flow rate of 100 sccm, a scan speed of 20 mm/min, and a feed pitch of 0.1 mm. Low surface roughness < 0.5 nmRMS was maintained over a wide range of removal depths up to $\sim$13 μm in both experiments. Tool marks were not observed in the scanned area owing to the small feed pitch. At a removal depth of $\sim$10 μm, the surface undulation and roughness of the processed area were $\sim$0.2 μm in PV and 0.4 nmRMS as respectively shown in **Figs. 9(b)** and **(c)**, which were much smaller than the target values. In addition, surface flatness can be improved by scanning the plasma with computer-controlled scan speeds.

4. Conclusion

As a high-precision inner-wall surface finishing method of CCMs with $W < 8$ mm, we developed an inner-wall PCVM method using two types of small electrodes. The removal rate of the $\phi 4$ cylindrical electrode for $W > 5$ mm was five times higher than that of the nozzle electrode. The nozzle electrode is available for the narrower channel of $W > 3$ mm, while it can generate the smaller plasma area of 0.7 mm, which is useful for precise correction of figure errors. The MRRs were independent on the lattice planes with a maximum error of 8.5%, while the av-

eraged relative standard deviation of MMRs was 3.2%. Using both electrodes, we succeeded in obtaining a sufficiently flat and smooth surface of < 1 μm in PV and < 1 nmRMS at the target removal depth of $\sim$10 μm for commercial Si wafers, which showed high feasibility to fabricate speckle-free CCMs for coherent X-ray applications.

References:

[1] P. Emma et al., "First lasing and operation of an ångstrom-wavelength free-electron laser," Nature Photon., Vol.4, pp. 641-647, 2010.

[2] T. Ishikawa et al., "A compact X-ray free-electron laser emitting in the sub-ångström region," Nature Photon., Vol.6, pp. 540-544, 2012.

[3] H. Fujimoto, A. Waseda, and X. Zhang, "Profile Measurement of Polished Surface with Respect to a Lattice Plane of a Silicon Crystal Using a Self-Referenced Lattice Comparator," Int. J. Automation Technol., Vol.5, No.2, pp. 179-184, 2013.

[4] M. Yabashi, K. Tamasaku, S. Kikuta, and T. Ishikawa, "X-ray monochromator with an energy resolution of 8×10^{-9} at 14.41 keV," Rev. Sci. Instrum., Vol.72, pp. 4080-4083, 2001.

[5] K. Tono et al., "Beamline, experimental stations and photon beam diagnostics for the hard x-ray free electron laser of SACLA," New J. Phys., Vol.15, pp. 083035, 2013.

[6] A. Diaz et al., "Coherence and wavefront characterization of Si-111 monochromators using double-grating interferometry," J. Synchrotron Rad., Vol.17, pp. 299-307, 2010.

[7] I. Sergueev, R. Döhrmann, J. Horbach, and J. Heuer, "Angular vibrations of cryogenically cooled double-crystal monochromators," J. Synchrotron Rad., Vol.23, pp. 1097-1103, 2016.

[8] U. Bonse and M. Hart, "Tailless x-ray single-crystal reflection curves obtained by multiple reflection," Appl. Phys. Lett., Vol.7, pp. 238-240, 1965.

[9] G. Faigel et al., "New Approach to the Study of Nuclear Bragg Scattering of Synchrotron Radiation," Phys. Rev. Lett., Vol.58, pp. 2699-2701, 1987.

[10] A. V. Zozulya et al., "Wavefront preserving channel-cut optics for coherent x-ray scattering experiments at the P10 beamline at PETRAIII," J. Phys. Conf. Ser., Vol.499, pp. 012003, 2014.

[11] P. K. Dhillon and S. Sarkar, "Non-monotonic roughening at early stages of isotropic silicon etching," Appl. Surf. Sci., Vol.284, pp. 569-574, 2013.

[12] Y. Mori, K. Yamauchi, K. Yamamura, and Y. Sano, "Development of plasma chemical vaporization machining," Rev. Sci. Instrum., Vol.71, pp. 4627-4632, 2000.

[13] T. Osaka et al., "Fabrication of ultrathin Bragg beam splitter by plasma chemical vaporization machining," Key Eng. Mater., Vol.523-524, pp. 40-45, 2012.

[14] T. Osaka et al., "A Bragg beam splitter for hard x-ray free-electron lasers," Opt. Express, Vol.21, pp. 2823-2831, 2013.

[15] T. Hirano et al., "Development of speckle-free channel-cut crystal optics using plasma chemical vaporization machining for coherent x-ray applications," Rev. Sci. Instrum., Vol.87, p. 063118, 2016.

[16] Y.-P. Zhao, J. T. Drotar, G.-C. Wang, and T.-M. Lu, "Roughening in Plasma Etch Fronts of Si(100)," Phys. Rev. Lett., Vol.82, pp. 4882-4885, 1999.

[17] T. Osaka et al., "Wavelength-tunable split-and-delay optical system for hard X-ray free-electron lasers," Opt. Express, Vol.24, pp. 9187-9201, 2016.

[18] T. Osaka et al., "Characterization of temporal coherence of hard X-ray free-electron laser pulses with single-shot interferograms," IUCrJ, Vol.4, pp. 728-733, 2017.

[19] T. Hirano et al., "Performance of a hard X-ray split-and-delay optical system with a wavefront division," J. Synchrotron Rad., Vol.25, pp. 20-25, 2018.

[20] H. Seidel, L. Csepregi, A. Heuberger, and H. Bäumgartel, "Anisotropic Etching of Crystalline Silicon in Alkaline Solutions," J. Electrochem. Soc., Vol.137, pp. 3612-3626, 1990.

Name:
Takashi Hirano

Affiliation:
Ph.D. Student, Department of Precision Science and Technology, Graduate School of Engineering, Osaka University

Address:
2-1 Yamada-oka, Suita, Osaka 565-0871, Japan
Brief Biographical History:
2016- Ph.D. Student, Osaka University
2017- Research Fellow, Japan Society for the Promotion of Science
Main Works:
● "Performance of a hard X-ray split-and-delay optical system with a wavefront division," J. Synchrotron Rad., Vol.25, pp. 20-25, 2018.
● "Development of speckle-free channel-cut crystal optics using plasma chemical vaporization machining for coherent x-ray applications," Rev. Sci. Instrum., Vol.87, p. 063118, 2016.
Membership in Academic Societies:
● Japan Society for Precision Engineering (JSPE)
● Japanese Society for Synchrotron Radiation Research (JSSRR)
● International Society for Optics and Photonics (SPIE)

Name:
Yuki Morioka

Affiliation:
Graduate Student, Department of Precision Science and Technology, Graduate School of Engineering, Osaka University

Address:
2-1 Yamada-oka, Suita, Osaka 565-0871, Japan
Brief Biographical History:
2017- Graduate Student, Osaka University
Membership in Academic Societies:
● Japan Society for Precision Engineering (JSPE)
● Japanese Society for Synchrotron Radiation Research (JSSRR)

Name:
Shotaro Matsumura

Affiliation:
Undergraduate Student, Department of Precision Science and Technology, Graduate School of Engineering, Osaka University

Address:
2-1 Yamada-oka, Suita, Osaka 565-0871, Japan
Brief Biographical History:
2018- Undergraduate Student, Osaka University

Name:
Yasuhisa Sano

Affiliation:
Associate Professor, Department of Precision Science and Technology, Graduate School of Engineering, Osaka University

Address:
2-1 Yamada-oka, Suita, Osaka 565-0871, Japan
Brief Biographical History:
2001- Visiting Researcher, RIKEN
2003 Received Ph.D. in Engineering from Osaka University
2004- Associate Professor, Osaka University
Main Works:
● "Development of array-type atmospheric-pressure RF plasma generator with electric on-off control for high-throughput numerically controlled processes," Rev. Sci. Instrum., Vol.87, p. 105121, 2016.
● "Planarization of SiC and GaN Wafers Using Polishing Technique Utilizing Catalyst Surface Reaction," ECS J. Solid State Sci. Technol., Vol.2, pp. N3028-N3035, 2013.
● "Fabrication of ultrathin and highly uniform silicon on insulator by numerically controlled plasma chemical vaporization machining," Rev. Sci. Instrum., Vol.78, p. 086102, 2007.
Membership in Academic Societies:
● Japan Society for Precision Engineering (JSPE)
● Japan Society of Applied Physics (JSAP)

Name:
Taito Osaka

Affiliation:
Special Postdoctoral Researcher, SPring-8 Center, RIKEN

Address:
1-1-1 Kouto, Sayo-cho, Sayo-gun, Hyogo 679-5148, Japan
Brief Biographical History:
2016 Received Ph.D. in Engineering from Osaka University
2016- Special Postdoctoral Researcher, SPring-8 Center, RIKEN
Main Works:
● "Characterization of temporal coherence of hard x-ray free-electron laser pulses with single-shot interferograms," IUCrJ, Vol.4, pp. 728-733, 2017.
● "Wavelength-tunable split-and-delay optical system for hard X-ray free-electron lasers," Opt. Express, Vol.24, pp. 9187-9201, 2016.
● "A Bragg beam splitter for hard x-ray free-electron lasers," Opt. Express, Vol.21, pp. 2823-2831, 2013.
Membership in Academic Societies:
● Japanese Society for Synchrotron Radiation Research (JSSRR)
● International Society for Optics and Photonics (SPIE)

Name:
Satoshi Matsuyama

Affiliation:
Assistant Professor, Department of Precision Science and Technology, Graduate School of Engineering, Osaka University

Address:
2-1 Yamada-oka, Suita, Osaka 565-0871, Japan
Brief Biographical History:
2007 Received Ph.D. in Engineering from Osaka University
2007- Assistant Professor, Osaka University
Main Works:
● "50-nm-resolution full-field X-ray microscope without chromatic aberration using total-reflection imaging mirrors," Sci. Rep., Vol.7, p. 46358, 2017.
● "Nearly diffraction-limited X-ray focusing with variable-numerical-aperture focusing optical system based on four deformable mirrors," Sci. Rep., Vol.6, p. 24801, 2016.
● "Trace element mapping of a single cell using a hard X-ray nanobeam focused by a Kirkpatrick-Baez mirror system," X-ray Spectroscopy, Vol.38, No.2, pp. 89-94, 2009.
Membership in Academic Societies:
● Japan Society for Precision Engineering (JSPE)
● Japanese Society for Synchrotron Radiation Research (JSSRR)

Name:
Kazuto Yamauchi

Affiliation:
Professor, Department of Precision Science and Technology, Graduate School of Engineering, Osaka University

Address:
2-1 Yamada-oka, Suita, Osaka 565-0871, Japan
Brief Biographical History:
1991 Received Ph.D. in Engineering from Osaka University
2003- Professor, Osaka University
Main Works:
● A. Isohashi, K. Yamauchi et al., "Chemical etching of silicon carbide in pure water by using platinum catalyst,"Appl. Phys. Lett., Vol.110, p. 201601, 2017.
● H. Mimura, K. Yamauchi et al., "Breaking the 10 nm barrier in hard-X-ray focusing," Nature Phys., Vol.6, No.2, pp. 122-125, 2010.
● K. Yamauchi et al., "Microstitching interferometry for x-ray reflective optics," Rev. Sci. Instrum., Vol.74, No.5, pp. 2894-2898, 2003.
Membership in Academic Societies:
● Japan Society for Precision Engineering (JSPE), Fellow
● Japanese Society for Synchrotron Radiation Research (JSSRR)
● Japan Society of Applied Physics (JSAP)
● Surface Science Society of Japan (SSSJ)
● International Society for Optics and Photonics (SPIE), Fellow
● Optical Society of America (OSA), Fellow

Name:
Makina Yabashi

Affiliation:
Group Director, SPring-8 Center, RIKEN

Address:
1-1-1 Kouto, Sayo-cho, Sayo-gun, Hyogo 679-5148, Japan
Brief Biographical History:
1996- Japan Synchrotron Radiation Research Institute
2007- SPring-8 Center, RIKEN
Main Works:
● T. Ishikawa, M. Yabashi et al., "A compact X-ray free-electron laser emitting in the sub-ångström region," Nature Photon., Vol.6, pp. 540-544, 2012.
Membership in Academic Societies:
● Japanese Society for Synchrotron Radiation Research (JSSRR)